https://doi.org/10.31925/farmacia.2024.5.17 **ORIGINAL ARTICLE**

ENHANCED CYTOTOXICITY OF IRINOTECAN ADSORBED ON MESOSTRUCTURED ALUMINOSILICATE MATRICES

LUMINITA CLAUDIA MICLEA [1,2], SILVIU NASTASE [3], LAURA BAJENARU [3], RAUL-AUGUSTIN MITRAN [4], CRISTIAN MATEI [3], FAWZIA SHA'AT [5], EUGEN RADU [6], MIHAELA G. MOISESCU [1, 2]*, DANIELA BERGER [3], TUDOR SAVOPOL [1,2]

[1]*Biophysics and Cellular Biotechnology Dept., "Carol Davila" University of Medicine and Pharmacy, 050474, Bucharest, Romania*
[2]*Excellence Centre for Research in Biophysics and Cellular Biotechnology, "Carol Davila" University of Medicine and Pharmacy, 050474, Bucharest, Romania*
[3]*Faculty of Chemical Engineering and Biotechnologies, National University for Science and Technology Politehnica of Bucharest, 011061, Bucharest, Romania*
[4]*"Ilie Murgulescu" Institute of Physical Chemistry, Romanian Academy, 060021, Bucharest, Romania*
[5]*National Institute for Chemical - Pharmaceutical Research and Development - ICCF, 031299, Bucharest, Romania*
[6]*Microbiology III Dept., "Carol Davila" University of Medicine and Pharmacy, 050098, Bucharest, Romania*

**corresponding author: mihaela.moisescu@umfcd.ro*

Manuscript received: June 2024

Abstract

Mesostructured silica, such as MCM-41 and SBA-15 and aluminosilicates have demonstrated good biocompatibility and are used as nanosized drug delivery systems (DDSs). Doping with aluminium modulates their physico-chemical properties. This study aimed to assess the metabolic impact of the 24 h or 48 h incubation of NIH3T3 murine fibroblastic cells with three categories of aluminium-doped MCM-41 and SBA-15 used as DDSs for the cytotoxic irinotecan. After 24 h, unloaded Al-doped DDSs at 90 μg/mL presented no toxic effects. Irinotecan release from DDSs followed a Fickian diffusion with various release profiles. Higher Al content led to higher residual drug amounts, while larger pore sizes resulted in faster desorption of irinotecan. Irinotecan loaded onto Al-doped DDSs decreased cell viability compared to irinotecan in solution. The MCM-based carriers demonstrated greater effectiveness in delivering irinotecan than SBA-based DDSs. The 48 h discontinuous exposure to irinotecan-loaded DDSs exhibited similar cytotoxicity to continuous exposure, suggesting a saturation of DDSs cellular uptake. Confocal microscopy revealed that DDSs were embedded in the cell membranes, supporting the hypothesis of an endocytosis-driven uptake. Our results showed that mesoporous aluminosilicates can augment intracellular irinotecan delivery as a Trojan horse.

Rezumat

Silicea mezostructurată, cum ar fi MCM-41 și SBA-15, și aluminosilicații prezintă o bună biocompatibilitate și sunt utilizați ca sisteme dimensiuni nanometrice pentru livrarea medicamentelor (DDS). Dopajul cu aluminiu modulează proprietățile fizico-chimice ale acestora. Acest studiu a avut ca scop evaluarea impactului metabolic al incubării timp de 24 sau 48 de ore a fibroblastelor de şoarece NIH3T3 cu trei categorii de MCM-41 și SBA-15 dopate cu aluminiu utilizate ca DDS pentru citotoxicul irinotecan. După 24 de ore, DDS-urile dopate cu Al (90 μg/mL) nu au prezentat efecte toxice. Eliberarea irinotecanului din DDS a urmat modelul difuziei Fick, cu diferite profiluri de eliberare. Conținutul mai mare de Al a dus la cantități mai mari de medicament rezidual în DDS, în timp ce dimensiunile mai mari ale porilor au dus la desorbția mai rapidă a irinotecanului. Irinotecanul încărcat pe DDS dopat cu Al a scăzut viabilitatea celulară comparativ cu irinotecanul în soluție. DDS-urile bazate pe MCM au demonstrat o eficacitate mai mare decât cele bazate pe SBA în livrarea intracelulară a irinotecanului. Expunerea discontinuă de 48 de ore la DDS încărcate cu irinotecan a prezentat citotoxicitate similară cu expunerea continuă, sugerând o saturație a captării celulare a DDS-urilor. Microscopia confocală a localizat DDS-urile încorporate în membranele celulare, susținând un mecanism de încorporare celulară prin endocitoză. Rezultatele noastre au arătat că aluminosilicații mezoporoşi pot fi folosiţi drept „cal troian" pentru a creşte livrarea intracelulară a irinotecanului.

Keywords: aluminium containing mesoporous silica, irinotecan delivery, fibroblast cytotoxicity, confocal microscopy

Introduction

Mesoporous materials have attracted significant attention for drug delivery [1-6] due to their unique properties, including high surface area, large pore volume and tuneable pore size [1, 7]. These are key parameters in developing efficient drug delivery systems (DDSs) with good storage capacity.

Among mesoporous materials, MCM-41 and SBA-15 types of silica are widely used as DDSs [8, 9]. Their good biocompatibility has been reported over time [10-14]. So far, numerous biologically active molecules have been embedded into the channels of mesoporous materials – *e.g.*, antibiotics [15-19], cytotoxic drugs such as irinotecan [20-25], 5-fluorouracil

[26], cisplatin [23, 24], or doxorubicin [27, 28], plant-based anti-inflammatory substances such as curcumin [29] or quercetin [30] or antibacterial molecules [30, 31]. When loaded into SBA-15 or MCM-41 materials, the drug cytotoxicity was augmented compared to the drug administered alone [24, 25, 32-34].

DDS properties can be further improved by doping with different ions, such as aluminium [13, 16, 19, 23, 35-37] making them attractive candidates for biomedical drug delivery applications.

In silico, *in vitro* and *in vivo* studies assess the efficacy of mesoporous MCM-41 and SBA-15-based DDSs doped with aluminium. These studies mainly measure drug loading efficiency, drug release kinetics, cellular uptake and cytotoxicity. Doping of DDSs with aluminium increased the drug loading capacity of the MCM-41-based DDSs and decreased the release kinetics of the encapsulated drug [23, 35]. *In vivo*, studies have shown that cytotoxic administration *via* DDSs produced fewer side effects (renal and liver toxicity) compared to the cytotoxic alone [24]. *In vivo*, the toxicity of the unloaded nanocarriers is influenced by their distribution in tissues, clearance, surface charge and size [38].

Although numerous studies on drug-loaded DDSs describe their physicochemical properties and biological effects, only a few formulations have reached the clinical trial stage of evaluation [39]. For example, oral administration in healthy humans of anti-inflammatory drugs such as ibuprofen on silica–lipid hybrid formulation [40], simvastatin on lipo-ceramic hybrids [41], or fenofibrate on mesoporous silica [42] revealed good tolerability and an augmented bioavailability compared to respective molecules administered individually.

Future research efforts should focus on optimising the synthesis conditions, fine-tuning pores' structure and volume and exploring novel doping strategies to enhance the performance of these materials further. Additionally, comprehensive preclinical studies and clinical trials are essential to validate their efficacy, safety and pharmacokinetics *in vivo*. Furthermore, the development of multifunctional DDSs with theragnostic capabilities could revolutionise the field of precision medicine.

Herein, we studied the biocompatibility and the cytotoxic efficiency of different formulations of aluminium-doped MCM-41 and SBA-15 carriers containing irinotecan. Irinotecan is a highly used standard drug in colorectal, lung and pancreatic cancer treatment [43], either delivered alone or in combination with other cytotoxic drugs such as 5-fluorouracil and leucovorin (FOLFIRI formulation) [44]. Intracellular carboxylesterases convert Irinotecan to its active metabolite 7-ethyl-10-hydroxycamptothecin (SN38), which is 200 - 2000 times more efficient than irinotecan [45]. Irinotecan cytotoxicity relies on the inhibition of topoisomerase I [46, 47], the DNA replication is thus stopped.

The enzymatic conversion into SN-38 glucuronide inactivates the SN38 [48]. Some of the most significant adverse effects of irinotecan (*e.g.*, diarrhoea, nausea, vomiting, alopecia, fatigue, diarrhoea and neutropenia) [49, 50] are due to the accumulation in the organism of SN38 and its inactivated form. Furthermore, patients having single nucleotide polymorphisms for conversion enzymes and drug transporters are at increased risk for neutropenia, and a reduced initial dose is recommended for these patients [48, 51].

As a key drug in cancer treatment management, irinotecan is a valuable therapeutic agent to which the DDS concept may be applied. Studies about the synthesis of mesoporous silica-based DDSs for this drug demonstrate that irinotecan may be successfully loaded into the mesopores of pristine and functionalised MCM-41 and SBA-15 [19, 25, 35, 52, 53].

The present study details the textural features of aluminium-doped MCM-41 and SBA-15 DDSs loaded with irinotecan and their cytotoxicity on NIH3T3 adherent murine fibroblastic cells. Furthermore, the localisation of fluorescently labelled SBA-15 within the cells is studied by confocal microscopy to unveil the mechanisms behind the cytotoxicity of irinotecan-loaded DDSs.

Materials and Methods

Materials and chemical reagents

Tetraethylorthosilicate (TEOS, Fluka), aluminium-tri-sec-butoxide ($Al(O^{sec}Bu)_3$, Sigma-Aldrich), aluminium sulphateoctadecahydrate ($Al_2(SO_4)_3 \cdot 18H_2O$, Sigma-Aldrich), trimethyl-tetradecyl ammonium bromide (C_{14}TAB, Fluka), trimethyl-hexadecylammonium bromide (C_{16}TAB, AlfaAesar), ammonia 25% (Scharlau), sulphuric acid 95 - 97% (Merck), N-buthyldiethanolamine (BuDEA, Aldrich), potassium dihydrogen phosphate (Merck), sodium hydrogen phosphate (Sigma-Aldrich), sodium chloride (Sigma-Aldrich), potassium chloride (Sigma-Aldrich), calcium chloride (Sigma-Aldrich), poly(ethylene glycol)-block-poly-(propylene glycol)-block-poly(ethylene glycol) (Pluronic P123, average MW 5800, Sigma-Aldrich), N-hydroxysuccinimide (HOSU, Fluka), anhydrous dimethylsulfoxide (DMSO, Sigma-Aldrich), (3-aminopropyl)-triethoxysilane (> 97%, Sigma-Aldrich), toluene anhydrous (99.7% Sigma-Aldrich, diisopropylcarbodiimide (DIC, Sigma-Aldrich) and irinotecan hydrochloride (Sigma-Aldrich) were used as received, without further purification. Zinc tetracarboxy phthalocyanine (ZnTCPC) was kindly offered by Dr. Aurel Diacon. The detailed synthesis procedure was described by Diacon A *et al.* [54]. All reagents were used as received without further purification.

Synthesis of DDSs

The mesoporous carriers were prepared by slightly modifying already reported procedures [15, 16]. Briefly, to obtain the AlMCM (13) support (AlMCM-41,

Si/Al ratio = 13), 25% (wt) aqueous ammonia solution (10 mL) was added to 120 mL solution containing 2.4 g C_{16}TAB in deionised water. Then, 1.435 mL N-butyldiethanolamine (BuDEA, organic additive) was introduced, followed by 10 mL TEOS and 0.298 g Al (O-sec-Bu) under magnetic stirring and an inert atmosphere. The resulting mixture was stirred at 40°C for 24 h and then hydrothermally treated at 150°C for 24 h. The solid product was filtered off, washed with ethanol, hot water and 0.1 M HCl, dried at room temperature and calcinated at 600°C for 5 h.

The synthesis of the AlMCM (51) support (AlMCM-41, Si/Al = 51) was similar to that of AlMCM (13), but instead of C16TAB, C14TAB was used without adding BuDEA.

The synthesis of SBA (SBA-15) and AlSBA (46) (AlSBA-15; Si/Al ratio = 46), using aluminium sulfate and, as template agent, Pluronic P123 (average MW 5800), was described elsewhere [16]. The synthesis of 3-aminopropyl functionalised SBA-15 was previously reported [55].

ZnTCPC was grafted onto SBA-APTES by the condensation reaction between carboxylic groups and aminopropyl moieties. SBA-APTES (103 mg) was added, at room temperature, to a 20 mL mixture of anhydrous DMSO containing N-hydroxysuccinimide (0.494 mM), DIC (0.495 mM) and ZnTCPC (0.123 mM). The reaction mixture was stirred for 18 h. The resulting solid was recovered by centrifugation, washed repeatedly with DMSO, water and 2-propanol, and dried under vacuum for 24 h. The resulting powder will be further referred to as SBA-Phtalo.

Characterisation of DDSs

The powders were analysed by small and wide-angle X-ray diffraction (XRD, Rigaku Mini Flex II diffractometer equipped with Cu-K_α monochromator). The differential scanning calorimetry (DSC) data were collected using a Setaram DSC 131 EVO calorimeter under nitrogen flow between 30°C and 300°C, with a heating rate of 10°C/min. The textural features of carriers without or with irinotecan were determined by measuring the nitrogen adsorption/desorption isotherms at 77 K (Quantachrome Autosorb iQ2 porosimeter). The Rigaku Sequential X-ray fluorescence spectrometer (ZSX Primus II) was used to determine the aluminosilicate samples' Si/Al molar ratio. Ultraviolet-visible (UV-Vis) spectra of solutions were recorded using an Ocean Optics USB 4000 spectrophotometer.

Drug adsorption on DDSs

Irinotecan loading was carried out using the solution impregnation procedure, as already reported [20, 55]. Briefly, the mesoporous supports (0.075 g), previously dried under vacuum, were suspended in 7.5 mL of 6.64 mg/mL drug acidic aqueous solution for 40 h at room temperature, under magnetic stirring (200 rpm). The drug-loaded samples were isolated by centrifugation, carefully washed with water, and dried under a vacuum. The drug content in the samples was monitored by measuring the supernatant absorption at 375 nm. The irinotecan-loaded materials are further referred to as iri@AlMCM (13), iri@AlMCM (51), iri@SBA and iri@AlSBA (46).

Drug release profiles from DDSs

The drug release profiles were determined in simulated biological fluids (water-based solutions prepared as previously mentioned [21, 56-58]): phosphate buffered solution (PBS, 8.01 mg/mL NaCl, 0.2 mg/mL KCl, 1.78 mg/mL $Na_2HPO_4 \cdot 2H_2O$, 0.27 mg/mL KH_2PO_4, adjusted to pH 5.7) and Ringer solution (8.60 mg/mL NaCl, 0.3 mg/mL KCl, 0.33 mg/mL $CaCl_2$). Briefly, *cca*. 15 mg of each irinotecan-loaded sample were dispersed individually in 1 mL of either PBS or Ringer, transferred in dialysis bags, and dialysed at 37°C against 90 mL of the respective PBS or Ringer solutions, under magnetic stirring (100 rpm) (dialysis tubing cellulose membrane, molecular weight cut-off 14000, Sigma-Aldrich). Periodically, small amounts of the release fluid were withdrawn and analysed by UV-Vis spectroscopy.

Preparation of DDS suspensions

Before each experiment, fresh DDSs stock suspensions of AlMCM (13), AlMCM (51), SBA, AlSBA (46) and their irinotecan-loaded counterparts were prepared using the following protocol: DDSs were sterilised by UV irradiation (1 h in the laminar flow hood), then suspended in sterile saline solution (146 mM NaCl, 2.6 mM KCl, 10.14 mM Na_2HPO_4, 1.76 mM KH_2PO_4 in ddH_2O, pH 7.4, 300 mOsm/kg), at 1 mg/mL, and vigorously dispersed on ice (1 h in ultrasonic bath, followed by 3-4 repeated cycles of vortexing at room temperature). The working suspensions were prepared by diluting the stock suspensions in a fresh culture medium. The concentrations of the various irinotecan-loaded carriers' suspensions in the culture medium were adjusted to have the same final amount of irinotecan (10 μg/mL). The concentration of each irinotecan-free carrier in the culture medium was 90 μg/mL. To check the cytotoxic effects of irinotecan on cells, an irinotecan solution (10 μg/mL) was prepared as previously described [20].

Cells incubation with DDSs

The fibroblasts murine adherent cell line NIH3T3 (CRL-1658, ATCC) was used. Cells were cultured in a humidified atmosphere at 37°C, 5% (vol.) CO_2, in Dulbecco's Modified Eagle's Essential Medium (DMEM) containing 4.5 g/L glucose, 100 mM L-glutamine, with phenol red (D-5796, Sigma-Aldrich), supplemented with 10% foetal bovine serum (FBS, F7524 Sigma-Aldrich), without antibiotics. Cells were seeded at equal concentrations in 24 wells plates (662160, Greiner BioOne, Cellstar) and grown for 24 h. Then, the culture medium was replaced with working suspensions of DDSs.

The cells were further incubated as follows: (a) for 24 h, (b) for 48 h and (c) for 24 h, after which the working suspension was replaced with a fresh medium,

and cells were further incubated for other 24 h (these experimental categories were named: 24 h, 48 h and 24 h ±, respectively). The cells were incubated with irinotecan in solution (10 µg/mL final concentration), with DDSs containing irinotecan (100 µg/mL final concentration), or with DDSs without irinotecan (90 µg/mL final concentration). Controls were cells cultured in a medium without DDS or irinotecan.

After the incubation, the cellular metabolic viability was assessed by CellTiter 96® AQueous One Solution Cell Proliferation Assay (MTS) (G3580, Promega), using a plate reader (Stat Fax 3200, Awareness Technology), according to the manufacturer's instructions. After the incubation, the medium containing DDSs or irinotecan was removed, and cells were washed three times with DMEM without phenol red (with 1 g/L glucose, without L-glutamine, 11054020, Gibco). Then, a freshly prepared mix of MTS and DMEM without phenol red (v/v ratio 1:5) was added to the wells, and cells were incubated for 2 h at 37°C, 5% (vol.) CO_2. The MTS tetrazolium compound is reduced by the dehydrogenase enzymes existing in metabolically active cells, producing a coloured formazan-based compound soluble in a culture medium. Afterwards, 150 mL from each well were transferred to a clean 96-well plate (92048, TPP), and formazan absorbance was measured at 492 nm. Viability is expressed as relative to the control averaged value. All data calculations and interpretations as graphs were done with Microsoft Excel and Origin™. Three to five independent experiments were carried out for each experimental category.

Confocal microscopy

NIH3T3 cells were cultivated for 24 h on coverslips (4000 cells *per* coverslip, Ø 24 mm) and then incubated with a suspension of SBA-Phtalo in DMEM (90 µg/mL) for 24 h, 48 h and 24 h ± in the same conditions as described above. The coverslips were then washed with DMEM without phenol red, and the cells were incubated for 30 min at 37°C with Rhodamine B (20 µg/mL, R-6626, Sigma-Aldrich) for membrane staining. Cells were then washed twice with DMEM without phenol red and incubated for 30 min at 37°C with Hoechst (2 µg/mL, 33342, Molecular Probes) for nuclear DNA staining (both dye solutions were freshly made in DMEM without phenol red). Every coverslip was washed twice with DMEM without phenol red and mounted on microscopy slides.

Images were acquired using the Zeiss LSM710 spectral system and Zeiss Zen v.10 software. Images were acquired separately for blue and red channels and superposed during digital processing.

The following wavelengths were used: for SBA-Phtalo λ_{ex} = 405 nm, λ_{em} = 690 - 740 nm, for Hoechst λ_{ex} = 405 nm, λ_{em} = 410 - 465 nm and for Rhodamine B λ_{ex} = 543 nm, λ_{em} = 590 - 650 nm. 40× and 63× immersion objectives and a confocal pinhole equivalent to 1 Airy Unit were used.

Image analysis was done using ImageJ and LSM Image Browser. SBA-Phtalo DDSs were digitally coloured in red, cell nuclei labelled with Hoechst in blue and membranes labelled with Rhodamine B in green.

Statistical analysis

Statistical significances were calculated using One way ANOVA (Origin™) and represented with black stars (* $p < 0.05$, ** $p < 0.01$, *** $p < 0.001$).

Results and Discussion

Characterisation of DDSs

Thermogravimetric analysis.

The phthalocyanine content was quantified by thermogravimetric analysis (Figure 1). The organic groups burn at temperatures higher than 250°C. For SBA-APTES, the 12.67% wt. mass loss corresponds to a molar ratio SiO_2:aminopropyl of 6.65:1, while the 20.82% wt. weight loss registered for SBA-Phtalo evidenced an incomplete condensation of aminopropyl groups with phthalocyanine dye in a molar ratio phthalocyanine:unreacted aminopropyl of 1:18.7. The low percentage of grafted dye can be explained by the steric hindrance caused by the bulky dye molecules inside the mesopores.

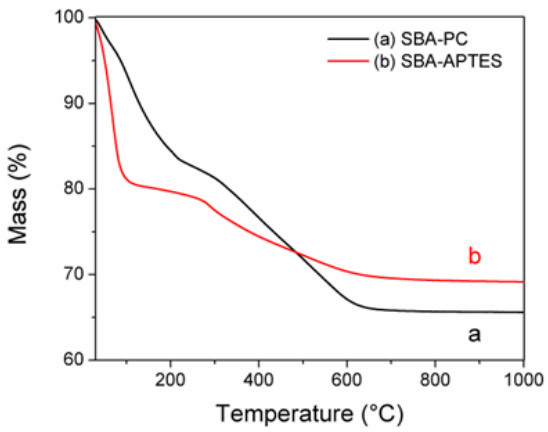

Figure 1.
Thermogravimetric analyses of SBA-Phtalo (a) and SBA-APTES (b)

Small- and wide-angle X-ray diffraction

Figure 2 displays the small-angle XRD patterns of the AlMCM-41 carriers. A higher aluminium content (red line) induced the formation of a less ordered mesophase, exhibiting broader and less intense diffraction peaks (110 and 200 Bragg reflections) compared to samples with less aluminium content (black line). SBA-APTES (Figure 2b, red line) and SBA-Phtalo (Figure 2b, black line) also show the 100, 110 and 200 Bragg reflections characteristic for P6mm hexagonal mesostructured materials.

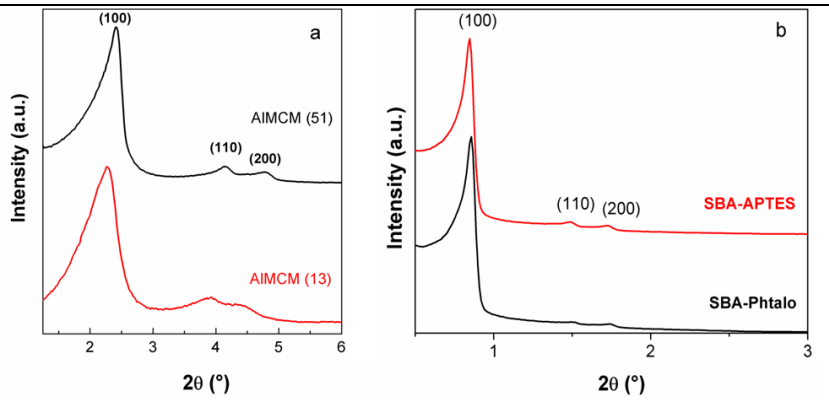

Figure 2.
Small-angle XRD patterns of (a) AlMCM (13) (red line) and AlMCM (51) (black line), (b) SBA-APTES (red line) and SBA-Phtalo (black line)

Small angle-XRD indicates highly ordered MCM-41 and SBA-15-type materials, regardless of the aluminium content in the silica matrix.

Wide-angle XRD patterns of the drug-loaded DDSs (Figure 3 traces a-d) are similar and dominated by a broad peak specific to amorphous materials, along with some low-intensity diffraction peaks. The latter suggests an incipient crystalline phase of irinotecan on the outer surface of the support, except for the iri@AlSBA (46) sample (Figure 3, trace d). Hence, the wide-angle XRD results support the prevalence of an amorphous irinotecan in the drug-loaded samples. As small-angle XRD showed, irinotecan, adsorbed in pores, affects the ordering of the mesophases. For instance, in the case of iri@SBA and iri@AlSBA (46) samples (Figure 3, traces e and f), the incorporation of irinotecan is accompanied by a decrease in the relative intensity of the 110 and 200 diffraction peaks. This is due to the pores' space filling with irinotecan, increasing the local electronic density [59].

Nitrogen adsorption/desorption isotherms

The N_2 sorption isotherm of the AlMCM-41(13) sample is presented in Figure 4a; the inset shows the corresponding pore size calculated using the Barrett-Joyner-Halenda model from the desorption branch (Table I).

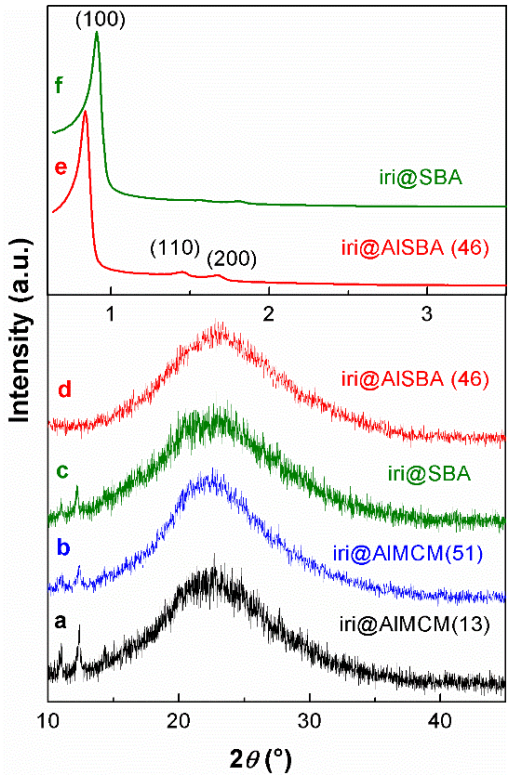

Figure 3.
XRD patterns of drug-loaded DDSs: small-angle (top, traces e, f) and wide-angle (bottom, traces a - d)

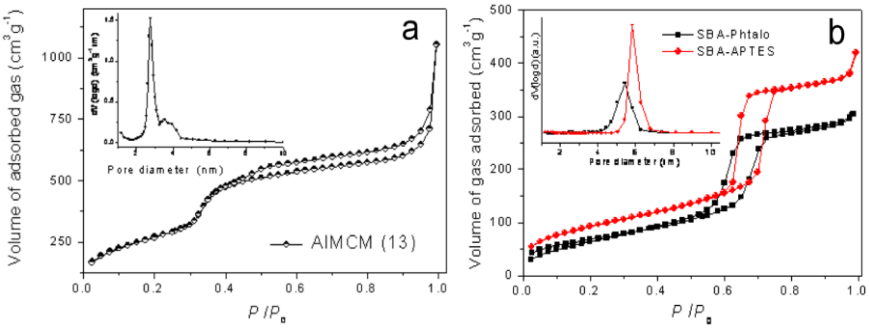

Figure 4.
Nitrogen adsorption/desorption isotherm for AlMCM (13) carrier (a) and SBA-Phtalo in comparison with SBA-APTES (b) (Inset: corresponding pore size distribution)

Various textural and structural parameters of DDSs and SBA-Phtalo: specific surface area (S_{BET}), average pore diameter (d_{BJH}), total pore volume (V_{pore}), spacing $d_{(100)}$ and unit cell parameter (a_0) were calculated based on adsorption/desorption isotherms (Table I and Table II).

To estimate the reservoir capability of the inorganic matrices, one can consider the values of the irinotecan uptake in the resulting drug-loaded materials. Considerable uptake values for all the studied mesoporous supports (around 35%) can be noticed (Table I). The irinotecan adsorption in the mesostructured frameworks is a complex phenomenon, and its mechanism can be regarded as a consequence of the synergy between the interactions occurring at the organic-inorganic assembly level and the porous nature of the platforms. Among the textural features, the specific surface area influences the drug loading most, resulting in higher irinotecan uptake values with S_{BET} increasing. Therefore, one can state that the studied inorganic matrices can act as reservoirs for irinotecan molecules.

For the SBA-Phtalo, based on N_2 adsorption/desorption isotherms (Figure 4b) lower pore size was calculated (compared to SBA-APTES) (Table II), indicating that the dye molecules are grafted on the inner surface of pore walls.

Table I

Textural parameters and irinotecan content in DDSs

Samples	S_{BET} [m2/g]	d_{BJH} [nm]	V_{pore} [cm3/g]	Irinotecan content in DDS [%wt]
AlMCM (13)	1001	2.77	1.63	36.1
AlMCM (51)	836	2.57	0.87	34.8
SBA	1055	6.26	1.50	36.1
AlSBA (46)	921	6.82	1.32	35.2

Table II

Structural and textural parameters for the mesoporous materials

Sample	$d_{(100)}$-spacing [nm]	a_0 [nm]	S_{BET} [m2/g]	d_{BJH} [nm]	V_{pore} [cm3/g]
SBA-APTES	10.40	12.00	340	5.83	0.59
SBA-Phtalo	10.32	11.80	250	5.43	0.48

Differential scanning calorimetry

DSC traces of the drug-loaded samples (Figure 5, traces b - e) were compared with that of the irinotecan hydrochloride solution (Figure 5, trace a). The aqueous solution of the drug displays two endothermic events associated with the loss of hydrochloric acid and adsorbed water molecules (at *cca*. 100°C) and the drug melting (T_{onset} = 270.3°C).

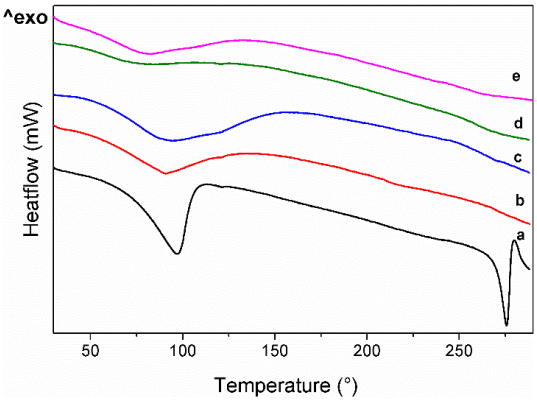

Figure 5.

DSC traces of irinotecan hydrochloride solution (trace a) and drug-loaded DDSs: iri@AlSBA (46) (b), iri@AlMCM (51) (c), iri@SBA (d) and iri@AlMCM (13) (e)

DSC traces of irinotecan-loaded carriers are dominated by the first broad endothermic event ascribed to the desorption of the adsorbed water molecules. No well-defined melting event can be noticed, indicating the anticancer agent's existence in drug-loaded powders, mainly in an amorphous state. However, a very small endothermic event could be observed in the vicinity of the irinotecan melting point, which could be related to the presence of a small amount of crystalline drug phase, in agreement with the wide-angle XRD analysis (Figure 3).

Drug release profiles

The drug release experiments were carried out in PBS (pH = 5.7) and Ringer solution (pH = 7.4). The justification of buffer choice resides in the following aspects: pH provided by phosphate buffer solution saline is comparable with that of late endosomes (vesicular structures involved in the cellular uptake of mesoporous silica nanoparticles) [60, 61] while the Ringer solution mimics the human plasma through its ionic strength [56, 57] and pH.

The Korsmeyer-Peppas model [62] is frequently used to characterise the delivery kinetics of drugs from mesoporous silica mathematically supported in various simulated body fluids [63, 64]**.** The model, which can be used for the analysis of the first 60% of the drug release curve, is described by the following power-law model equation [58]:

$$M_t/M_\infty = kt^n$$

where, M_t represents the cumulative released drug mass at a particular moment *t*, M_∞ stands for the total amount of irinotecan in the initial sample, and *n* is an exponent indicating the type of mechanism involved in the desorption process. When n = 0.5, a Fickian diffusion mechanism is engaged, whereas n > 0.5

corresponds to a non-Fickian delivery. The release constant, *k*, contains information about the tortuosity and porosity of the matrix, the diffusivity and the solubility of the drug, or the total amount of the drug retained in the carrier. Larger values of *k* suggest faster desorption rates.

In Figure 6, the release curves of irinotecan from all the DDS categories, suspended in PBS and Ringer solutions, are presented.

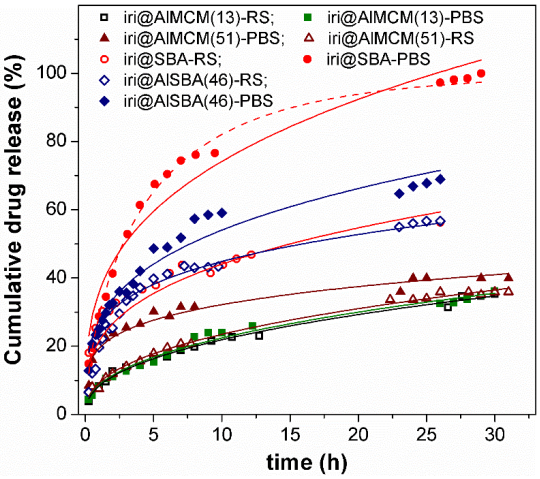

Figure 6.
Irinotecan release profiles
The continuing lines represent the fitted experimental data using the Korsmeyer-Peppas equation, while the dashed red curve represents the fit using the Weibull model.

An incomplete release of irinotecan from all used carriers, except for iri@SBA (red-filled circles) in PBS, was noticed in both buffers (**Error! Reference s ource not found.**). For the drug-loaded carriers based on AlMCM-41, suspended either in PBS (iri@AlMCM (13) and iri@AlMCM (51) - green filled squares and brown filled triangle, respectively) or in Ringer (iri@AlMCM (13) and iri@AlMCM (51) - black open squares and open brown triangles, respectively), the residual amount of irinotecan can be related to the aluminium content of support, being positively correlated with the amount of Al in the carrier. This tendency originates from the strong interactions between drug molecules and the acidic surface of the carriers, reinforcing the stability of the drug-support assembly.

Faster release kinetics of irinotecan were observed in PBS for DDSs containing less aluminium (iri@AlMCM (51) and iri@SBA samples, compared to iri@AlMCM (13) and iri@AlSBA, respectively) (Figure 6, brown-filled triangles and red-filled circles, respectively, and corresponding *k* values in Table III). This behaviour is more pronounced for iri@SBA, for which the release completes after 30 h. The absence of a residual amount of drug in this last case could be related to the larger pore size of the support, which allows for better mobility of host molecules in the guest framework and weaker irinotecan-silica matrix interactions.

Considering that, in our release experiments, the cumulative irinotecan release is smaller than 60% (except for the iri@SBA sample in PBS), it was possible to properly fit the experimental data using the Korsmeyer-Peppas equation. For iri@SBA, delivery experimental data were better fitted by the Weibull model (dashed red curve in Figure 6), a two-parameter exponential function, which can be used for cumulative release amounts up to 90% [65]. Because values of *n* lower than 0.5 were obtained with high correlation coefficients (Table III), it is possible to assume that the irinotecan desorption from the studied inorganic matrices involved a Fickian diffusion mechanism. Also, the *k* values (Table III) agree with the experimental observations.

Table III

Estimated parameters of the Korsmeyer-Peppas model used for the description of irinotecan release

Sample	Ringer solution			PBS, pH = 5.7		
	k	***n***	**R^2**	***k***	***n***	**R^2**
iri@AlMCM (13)	8.33	0.42	0.99	8.58	0.42	0.98
iri@AlMCM (51)	9.32	0.40	0.99	19.40	0.22	0.95
iri@SBA	26.17	0.23	0.97	35.78	0.32	0.95
iri@AlSBA (46)	21.46	0.31	0.95	27.49	0.29	0.96

Cell viability assessment

The NIH3T3 cells were treated with irinotecan solution, irinotecan-loaded DDSs and their unloaded counterparts. The cell viability was assessed using the MTS assay (Figure 7).

For cells incubated 24 h with unloaded DDSs doped or not with aluminium, the cells' viability was not significantly altered. For exposures longer than 24 h (continuous or discontinuous), the unloaded carriers remained nontoxic except for AlSBA (46), which decreased, statistically significant, the cell viability concerning the control (Figure 7, traces b - c, AlSBA (46) boxes).

The toxic effect of irinotecan in solution, reflected by inhibition of approximately 60% of cellular viability (compared to control), was observed either in the case of 48 h continuous (Figure 7), trace c, irinotecan box) or discontinuous 24 h ± exposures (Figure 7, trace b, irinotecan box). It can observed that the viability measured immediately after 24 h of drug exposure (Figure 7, trace an irinotecan box) is not modified. The cells exposed to the drug for 24 h and then kept for another 24 h in a culture medium

without irinotecan (24 h ±) showed a viability similar to that of cells exposed 48 h continuously to irinotecan (Figure 7, traces b and c, irinotecan boxes). A possible explanation for this behaviour is that, as SN-38 forms and topoisomerase I is inhibited, cells stop their division cycle while entering the S phase. This process requires more than 24 h. The delayed cellular response to irinotecan has been observed in other studies [25].

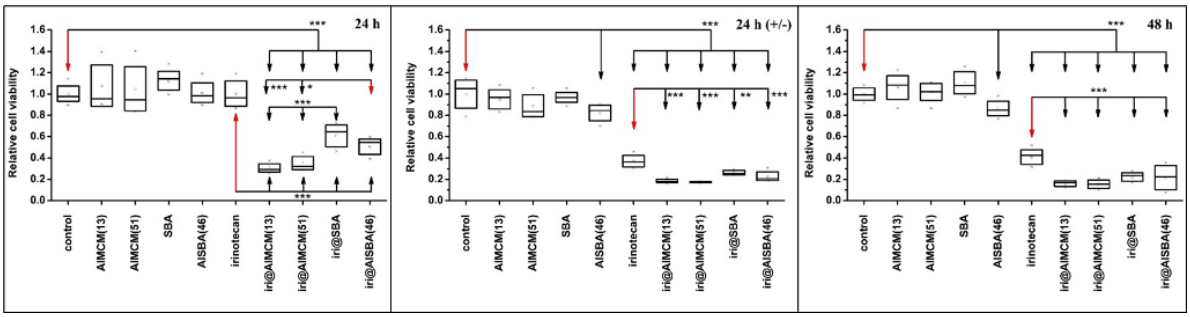

Figure 7.
Viability of NIH3T3 cells for different time incubations
The red arrows indicate the experimental category for the statistical comparison

The irinotecan-loaded DDSs were highly cytotoxic (Figure 7, traces a-c, iri@AlMCM (13), iri@AlMCM (51), iri@SBA and iri@AlSBA (46) boxes) compared to the control or irinotecan solution for all incubation times.

For 24 h exposure, iri@AlMCM (13) and iri@AlMCM (51) exhibited higher toxicity than iri@SBA and iri@AlSBA (46) (statistical significance indicated in Figure 7, trace a). This correlates with the irinotecan release profiles that showed slower kinetics for iri@AlMCM (13) and iri@AlMCM (51) compared to those for iri@SBA and iri@AlSBA (46) (as seen in Table III, *k* and *n* coefficients). Therefore, the iri@AlMCM (13) and iri@AlMCM (51) DDSs were provided with the necessary time to enter the cell before releasing a significant amount of cytotoxic, thus ensuring a higher intracellular irinotecan concentration.

For continuous or discontinuous 48 h incubations, the difference in irinotecan toxicity "delivered" by MCM and SBA-based carriers was no longer observed (Figure 7, traces b-c); moreover, the overall values of relative cell viability decreased to around 20% from the control value. When the incubation times are long, the irinotecan effect is high and similarly toxic regardless of the mesoporous carrier.

Removing the medium containing DDSs after 24 h of exposure (24 h ± experimental category) led to the same cellular proliferation pattern observed for the 48 h continuous exposure. This may suggest that the endocytosis process (supporting the DDSs cell entry) has reached a saturation level at 24 h.

While short-term (such as 24 h) *in vitro* studies have generally indicated low cytotoxicity of SBA-15 and MCM-41 at concentrations up to 2 mg/mL [66], there are still some concerns regarding the potential long-term effects and systemic toxicity. To evaluate the safety profile of SBA-15 and MCM-41 for biomedical applications, further investigations are recommended for advanced 3D cell culture models and *in vivo* assays.

Confocal microscopy

The localisation of the phthalocyanine moiety is fluorescently signalled either within the cell volume, as revealed by the orthogonal projections on the z-axis of the z-stack images (red conglomerates in Figure 8, traces b-c, white arrows), or embedded in the green signal of the membranes (red conglomerates in Figure 8, traces b-c, red arrows).

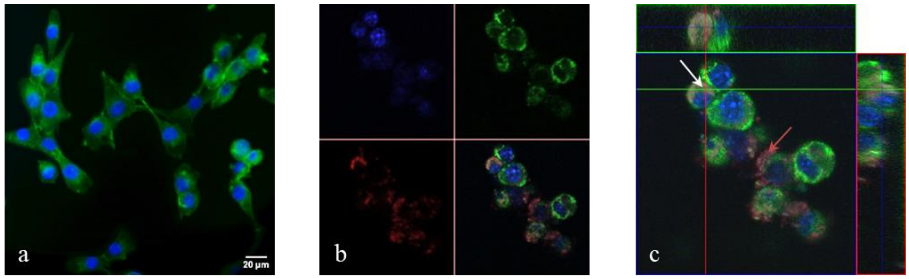

Figure 8.
Example of confocal microscopy images of NIH3T3 cells incubated with SBA-Phtalo DDSs
(a) control cells; (b) cells incubated with SBA-Phtalo for 48 h; (c) orthogonal projections on z-axis of the z-stack images focused on an SBA-Phtalo conglomerate localised inside the cell (white arrow); the conglomerates situated outer of the cell membrane are indicated by red arrow

Rhodamine B is a non-specific marker for both plasmalemma and endo-membranes. Therefore, the red SBA-Phtalo aggregates localised within a green background support the endocytosis-based uptake proposed for the internalisation of mesoporous silica DDSs in agreement with previous reports [60, 67]. The precise intracellular distribution of SBA-Phtalo DDSs was challenging to assess due to the lack of endosome-specific markers. The images acquired for 24 h and 24 (±) h (data not shown) showed a similar distribution of the DDSs.

Conclusions

The ordered mesoporous silica and aluminosilicate carriers used as DDSs were proven to be efficient reservoirs for irinotecan. The release of irinotecan from the mesostructured carriers followed mainly a Fickian diffusion process, and the corresponding release profiles depended on the carrier's physicochemical properties. A higher aluminium content in the mesoporous matrix generated more residual drug amount due to stronger drug-carrier interactions, while larger pore size induced faster desorption of irinotecan.

The cellular viability tests performed on NIH3T3 cultured cells indicated no toxic effects for proposed carriers at 90 μg/mL, regardless of duration and type of incubation (continuous or discontinuous), except for AlSBA (46), which presented a toxic effect seen at 48 h (continuous or discontinuous incubation).

Compared with irinotecan in solution (10 μg/mL), irinotecan loaded on aluminium-containing carriers decreased the cell viability the most, regardless of time and type of incubation. Therefore, the effectiveness of the irinotecan is augmented by its delivery *via* mesoporous aluminosilicates and silica matrices. MCM-41-based carriers were more effective in delivering the irinotecan than SBA-15-based DDSs at 24 h of continuous incubation; differences were no longer visible for 48 h exposures (continuous or discontinuous).

The discontinuous exposure to iri@DDSs (24 h ±) revealed similar cytotoxicity as the continuous one (48 h), supporting the hypothesis of DDSs uptake saturation.

The confocal microscopy images showed that the mesoporous carriers are embedded in membranes, often in conglomerates, possibly in correlation with endocytotic trafficking. These images suggest that the studied mesoporous DDSs augmented the intracellular irinotecan concentrations.

Acknowledgement

This work benefited from the partial financial support of research grants POSCCE-O2.1.2-2009-2, ID 691 and PCCA no. 131/2012.

Conflict of interest

The authors declare no conflict of interest.

References

1. Niculescu VC, Mesoporous Silica Nanoparticles for Bio-Applications. *Front Mater.*, 2020; 7.
2. Dutta Gupta Y, Mackeyev Y, Krishnan S, Bhandary S, Mesoporous silica nanotechnology: promising advances in augmenting cancer theranostics. *Cancer Nanotechnol.*, 2024; 15(1): 9.
3. Kannan K, Using Smart Mesoporous Silica in Designing Drug Delivery Systems. In Handbook of Smart Materials, Technologies and Devices, Hussain, C.M., Di Sia, P., Eds., *Springer International Publishing: USA*, 2022, 1581-1612.
4. Vallet-Regí M, Colilla M, Izquierdo-Barba I, Manzano M, Mesoporous Silica Nanoparticles for Drug Delivery: Current Insights. *Molecules*, 2017; 23(1): 47.
5. Trzeciak K, Chotera-Ouda A, Bak-Sypien II, Potrzebowski MJ, Mesoporous Silica Particles as Drug Delivery Systems - The State of the Art in Loading Methods and the Recent Progress in Analytical Techniques for Monitoring These Processes. *Pharmaceutics*, 2021; 13(7): 950.
6. Yao Y, Zhou Y, Liu L, Xu Y, Chen Q, Wang Y, Wu S, Deng Y, Zhang J, Shao A, Nanoparticle-Based Drug Delivery in Cancer Therapy and Its Role in Overcoming Drug Resistance. *Front Mol Biosci.*, 2020; 7: 193.
7. Zhao D, Huo Q, Feng J, Chmelka BF, Stucky GD, Nonionic Triblock and Star Diblock Copolymer and Oligomeric Surfactant Syntheses of Highly Ordered, Hydrothermally Stable, Mesoporous Silica Structures. *J Am Chem Soc.*, 1998; 120(24): 6024-6036.
8. Chaudhary V, Sharma S, An overview of ordered mesoporous material SBA-15: synthesis, functionalization and application in oxidation reactions. *J Por Mat.*, 2017; 24(3): 741-749.
9. Jarmolińska S, Feliczak-Guzik A, Nowak I, Synthesis, Characterization and Use of Mesoporous Silicas of the Following Types SBA-1, SBA-2, HMM-1 and HMM-2. *Materials*, 2020; 13(19): 4385.
10. Vivero-Escoto JL, Slowing II, Trewyn BG, Lin VS-Y, Mesoporous Silica Nanoparticles for Intracellular Controlled Drug Delivery. *Small*, 2010; 6(18): 1952-1967.
11. Tang F, Li L, Chen D, Mesoporous Silica Nanoparticles: Synthesis, Biocompatibility and Drug Delivery. *Adv Mat.*, 2012; 24(12): 1504-1534.
12. Tarn D, Ashley CE, Xue M, Carnes EC, Zink JI, Brinker CJ, Mesoporous Silica Nanoparticle Nanocarriers: Biofunctionality and Biocompatibility. *Acc Chem Res.*, 2013; 46(3): 792-801.
13. Zhang C, Xie H, Zhang Z, Wen B, Cao H, Bai Y, Che Q, Guo J, Su Z, Applications and Biocompatibility of Mesoporous Silica Nanocarriers in the Field of Medicine. *Front Pharmacol.*, 2022; 13.
14. Bajenaru L, Berger D, Miclea L, Matei C, Nastase S, Andronescu C, Moisescu MG, Savopol T, Correlation of the intracellular reactive oxygen species levels with textural properties of functionalised mesostructured

silica. *J Biomed Mater Res A.*, 2014; 102(12): 4435-4442.
15. Nastase S, Bajenaru L, Matei C, Mitran RA, Berger D, Ordered mesoporous silica and aluminosilicate-type matrix for amikacin delivery systems. *Micropor Mesopor Mat.*, 2013; 182: 32-39.
16. Berger D, Bajenaru L, Nastase S, Mitran R-A, Munteanu C, Matei C, Influence of structural, textural and surface properties of mesostructured silica and aluminosilicate carriers on aminoglycoside uptake and *in vitro* delivery. *Micropor Mesopor Mat.*, 2015; 206(C): 150-160.
17. Mitran R, Doxycycline encapsulation studies into mesoporous sba-15 silica type carriers and *in vitro* release. *Int Multidiscip Sci GeoConf Survey Geol Mining Ecology Manag, SGEM.*, 2014; 1(6): 53-60.
18. Dolete G, Purcăreanu B, Mihaiescu DE, Ficai D, Oprea OC, Bîrcă AC, Chircov C, Vasile BS, Vasilievici G, Ficai A, Andronescu E, A Comparative Loading and Release Study of Vancomycin from a Green Mesoporous Silica. *Molecules*, 2022; 27(17): 5589.
19. Berger D, Nastase S, Mitran RA, Petrescu M, Vasile E, Matei C, Negreanu-Pîrjol T, Mesostructured silica and aluminosilicate carriers for oxytetracycline delivery systems. *Int J Pharm.*, 2016; 510(2): 524-531.
20. Nastase S, Bajenaru L, Berger D, Matei C, Moisescu MG, Constantin D, Savopol T, Mesostructured silica matrix for irinotecan delivery systems. *Open Chem.*, 2014; 12(8): 813-820.
21. Ghimpău V, Sur D, Volovăț SR, Cazacu IM, Croitoru VM, Turcu-Știolică A, Gheonea DI, Tăerel AE, Subțirelu MS, Lungulescu CV, The direct costs burden of bevacizumab in South-West Romania. *Farmacia*, 2022; 70(1): 164-170.
22. Alkafajy AM, Albayati TM, High performance of magnetic mesoporous modification for loading and release of meloxicam in drug delivery implementation. *Mater Today Commun.*, 2020; 23: 100890.
23. Carmona FJ, Jiménez-Amezcua I, Rojas S, Romão CC, Navarro JAR, Maldonado CR, Barea E, Aluminum Doped MCM-41 Nanoparticles as Platforms for the Dual Encapsulation of a CO-Releasing Molecule and Cisplatin. *Inorg Chem.*, 2017; 56(17): 10474-10480.
24. Drača D, Edeler D, Saoud M, Dojčinović B, Dunđerović D, Đmura G, Maksimović-Ivanić D, Mijatović S, Kaluđerović GN, Antitumor potential of cisplatin loaded into SBA-15 mesoporous silica nanoparticles against B16F1 melanoma cells: *in vitro* and *in vivo* studies. *J Inorg Biochem.*, 2021; 217: 111383.
25. Miclea LC, Mihailescu M, Tarba N, Brezoiu AM, Sandu AM, Mitran RA, Berger D, Matei C, Moisescu MG, Savopol T, Evaluation of intracellular distribution of folate functionalised silica nanoparticles using fluorescence and hyperspectral enhanced dark field microscopy. *Nanoscale*, 2022; 14(35): 12744-12756.
26. Rehman F, Khan AJ, Sama ZU, Alobaid HM, Gilani MA, Safi SZ, Muhammad N, Rahim A, Ali A, Guo J, Arshad M, Surface engineered mesoporous silica carriers for the controlled delivery of anticancer drug 5-fluorouracil: Computational approach for the drug-carrier interactions using density functional theory. *Front Pharmacol.*, 2023; 14.
27. Wu M, Lin X, Tan X, Li J, Wei Z, Zhang D, Zheng Y, Zheng AX, Zhao B, Zeng Y, Liu X, Liu J, Photoresponsive Nanovehicle for Two Independent Wavelength Light-Triggered Sequential Release of P-gp shRNA and Doxorubicin To Optimize and Enhance Synergistic Therapy of Multidrug-Resistant Cancer. *ACS Appl Mater Interfaces.*, 2018; 10(23): 19416-19427.
28. Zaltariov MF, Ciubotaru BI, Ghilan A, Peptanariu D, Ignat M, Iacob M, Vornicu N, Mucoadhesive Mesoporous Silica Particles as Versatile Carriers for Doxorubicin Delivery in Cancer Therapy. *Int J Mol Sci.*, 2023; 24(19): 14687.
29. Atiyah NA, Albayati TM, Atiya MA, Functionalization of mesoporous MCM-41 for the delivery of curcumin as an anti-inflammatory therapy. *Adv Powder Tech.*, 2022; 33(2): 103417.
30. Alharthi S, Ziora ZM, Janjua T, Popat A, Moyle PM, Formulation and Biological Evaluation of Mesoporous Silica Nanoparticles Loaded with Combinations of Sortase A Inhibitors and Antimicrobial Peptides. *Pharmaceutics*, 2022; 14(5): 986.
31. Li C, Mo Y, Jiao L, Liu Y, Li X, Synthesis and Characterization of Mesoporous Silica Nanoparticles Loaded with P-Cymene against Rice Bacterial Blight. *Nanomaterials*, 2024; 14(3): 250.
32. Tao Z, Toms B, Goodisman J, Asefa T, Mesoporous Silica Microparticles Enhance the Cytotoxicity of Anticancer Platinum Drugs. *ACS Nano.*, 2010; 4(2): 789-794.
33. Almáši M, Beňová E, Zeleňák V, Madaj B, Huntošová V, Brus J, Urbanová M, Bednarčík J, Hornebecq V, Cytotoxicity study and influence of SBA-15 surface polarity and pH on adsorption and release properties of anticancer agent pemetrexed. *Mat Sci Eng C.*, 2020; 109: 110552.
34. Niroumand U, Firouzabadi N, Goshtasbi G, Hassani B, Ghasemiyeh P, Mohammadi-Samani S, The effect of size, morphology and surface properties of mesoporous silica nanoparticles on pharmacokinetic aspects and potential toxicity concerns. *Front Mater.*, 2023; 10: 1-5.
35. Mitran RA, Berger D, Pandele-Cusu J, Matei C, Effect of Aluminum Incorporation into Mesoporous Aluminosilicate Framework on Drug Release Kinetics. *J Nanomater.*, 2017; 2017: 1-9.
36. Ahmed K, Rehman F, Pires CTGVMT, Rahim A, Santos AL, Airoldi C, Aluminum doped mesoporous silica SBA-15 for the removal of remazol yellow dye from water. *Micropor Mesopor Mat.*, 2016; 236: 167-175.
37. Bajenaru L, Nastase S, Matei C, Berger D, Effect of aluminum content from mcm-41-type silica materials on the irinotecan adsorption and its *in vitro* release. *Rev Roum Chim.*, 2013; 58(9): 815-821.
38. Rosenholm JM, Sahlgren C, Lindén M, Towards multifunctional, targeted drug delivery systems using mesoporous silica nanoparticles - opportunities and challenges. *Nanoscale*, 2010; 2(10): 1870.
39. Janjua TI, Cao Y, Yu C, Popat A, Clinical translation of silica nanoparticles. *Nat Rev Mater.*, 2021; 6(12): 1072-1074.
40. Tan A, Eskandar NG, Rao S, Prestidge CA, First in man bioavailability and tolerability studies of a silica-

lipid hybrid (Lipoceramic) formulation: A Phase I study with ibuprofen. *Drug Deliv Transl Res.*, 2014; 4(3): 212-221.
41. Meola TR, Abuhelwa AY, Joyce P, Clifton P, Prestidge CA, A safety, tolerability, and pharmacokinetic study of a novel simvastatin silica-lipid hybrid formulation in healthy male participants. *Drug Deliv Transl Res.*, 2021; 11(3): 1261-1272.
42. Bukara K, Schueller L, Rosier J, Martens MA, Daems T, Verheyden L, Eelen S, Van Speybroeck M, Libanati C, Martens JA, Guy Van Den Mooter G, Frérart F, Jolling K, De Gieter M, Bugarski B, Kiekens F, Ordered mesoporous silica to enhance the bioavailability of poorly water-soluble drugs: Proof of concept in man. *Eur J Pharm Biopharm.*, 2016; 108: 220-225.
43. Kawai S, Takeshima N, Hayasaka Y, Notsu A, Yamazaki M, Kawabata T, Yamazaki K, Mori K, Yasui H, Comparison of irinotecan and oxaliplatin as the first-line therapies for metastatic colorectal cancer: a meta-analysis. *BMC Cancer.*, 2021; 21(1): 116.
44. Zhang X, Duan R, Wang Y, Liu X, Zhang W, Zhu X, Chen Z, Shen W, He Y, Wang H, Huang M, Wang C, Zhang Z, Zhao X, Qiu L, Luo J, Sheng X, Guo W, FOLFIRI (folinic acid, fluorouracil and irinotecan) increases not efficacy but toxicity compared with single-agent irinotecan as a second-line treatment in metastatic colorectal cancer patients: a randomised clinical trial. *Ther Adv Med Oncol.*, 2022; 14: 175883592110687.
45. Zhang JA, Xuan T, Parmar M, Ma L, Ugwu S, Ali S, Ahmad I, Development and characterization of a novel liposome-based formulation of SN-38. *Int J Pharm.*, 2004; 270(1-2): 93-107.
46. Hsiang YH, Hertzberg R, Hecht S, Liu LF, Camptothecin induces protein-linked DNA breaks *via* mammalian DNA topoisomerase I. *J Biol Chem.*, 1985; 260(27): 14873-14878.
47. Hsiang YH, Lihou MG, Liu LF, Arrest of replication forks by drug-stabilised topoisomerase I-DNA cleavable complexes as a mechanism of cell killing by camptothecin. *Cancer Res.*, 1989; 49(18): 5077-5082.
48. De Man FM, Goey AKL, Schaik RHN van, Mathijssen RHJ, Bins S, Individualization of Irinotecan Treatment: A Review of Pharmacokinetics, Pharmacodynamics and Pharmacogenetics. *Clin Pharmacokinet.*, 2018; 57(10): 1229-1254.
49. Fujita K, Irinotecan, a key chemotherapeutic drug for metastatic colorectal cancer. *World J Gastroenterol.*, 2015; 21(43): 12234.
50. Townsend D, Irinotecan. In xPharm: The Comprehensive Pharmacology Reference, Enna SJ, Bylund DB, Eds., *Elsevier Inc.: USA*, 2008, 1-5.
51. O'Dwyer PJ, Catalano R, Uridine Diphosphate Glucuronosyltransferase (UGT) 1A1 and Irinotecan: Practical Pharmacogenomics Arrives in Cancer Therapy. *J Clin Oncol.*, 2006; 24(28): 4534-4538.
52. Jiao Z, Chen Y, Wan Y, Zhang H, Anticancer efficacy enhancement and attenuation of side effects of doxorubicin with titanium dioxide nanoparticles. *Int J Nanomed.*, 2011; 6: 2321.
53. Fatemi M, Meshkini A, Matin MM, A dual catalytic functionalised hollow mesoporous silica-based nano-carrier coated with bacteria-derived exopolysaccharides for targeted delivery of irinotecan to colorectal cancer cells. *Int J Biol Macromol.*, 2024; 259: 129179.
54. Diacon A, Rusen E, Boscornea C, Zaharia C, Cincu C, Hybrid dye sensitised solar cells. *J Optoel Adv Mat.*, 2010; 12: 199-204.
55. Mitran R-A, Berger D, Băjenaru L, Năstase S, Andronescu C, Matei C, Azobenzene functionalised mesoporous AlMCM-41-type support for drug release applications. *Open Chem.*, 2014; 12(7): 788-795.
56. Souris JS, Lee C-H, Cheng S-H, Chen C-T, Yang C-S, Ho JA, Mou CY, Lo L, Surface charge-mediated rapid hepatobiliary excretion of mesoporous silica nanoparticles. *Biomaterials*, 2010; 31(21): 5564-5574.
57. Innes E, Yiu HHP, McLean P, Brown W, Boyles M, Simulated biological fluids - a systematic review of their biological relevance and use in relation to inhalation toxicology of particles and fibres. *Crit Rev Toxicol.*, 2021; 51(3): 217-248.
58. Maria G, Berger D, Nastase S, Luta I, Kinetic studies on the irinotecan release based on structural properties of functionalised mesoporous-silica supports. *Micropor Mesopor Mat.*, 2012; 149(1): 25-35.
59. Impéror-Clerc M, Davidson P, Davidson A, Existence of a Microporous Corona around the Mesopores of Silica-Based SBA-15 Materials Templated by Triblock Copolymers. *J Am Chem Soc.*, 2000; 122(48): 11925-11933.
60. Behzadi S, Serpooshan V, Tao W, Hamaly MA, Alkawareek MY, Dreaden EC, Brown D, Alkilany AM, Farokhzad OC, Mahmoudi M, Cellular uptake of nanoparticles: journey inside the cell. *Chem Soc Rev.*, 2017; 46(14): 4218-4244.
61. Noureddine A, Paffett ML, Franco S, Chan AE, Pallikkuth S, Lidke K, Serda RE, Endolysosomal Mesoporous Silica Nanoparticle Trafficking along Microtubular Highways. *Pharmaceutics*, 2021; 14(1): 56.
62. Korsmeyer RW, Gurny R, Doelker E, Buri P, Peppas NA, Mechanisms of solute release from porous hydro-philic polymers. *Int J Pharm.*, 1983; 15(1): 25-35.
63. Qu F, Zhu G, Huang S, Li S, Qiu S, Effective Controlled Release of Captopril by Silylation of Mesoporous MCM-41. *Chem Phys Chem.*, 2006; 7(2): 400-406.
64. Wang S, Ordered mesoporous materials for drug delivery. *Micropor Mesopor Mat.*, 2009; 117(1-2): 1-9.
65. Papadopoulou V, Kosmidis K, Vlachou M, Macheras P, On the use of the Weibull function for the discernment of drug release mechanisms. *Int J Pharm.*, 2006; 309(1-2): 44-50.
66. Heikkilä T, Santos HA, Kumar N, Murzin DY, Salonen J, Laaksonen T, Peltonen L, Hirvonen J, Lehto VP, Cytotoxicity study of ordered mesoporous silica MCM-41 and SBA-15 microparticles on Caco-2 cells. *Eur J Pharma Biopharm.*, 2010; 74(3): 483-494.
67. Tao Z, Toms BB, Goodisman J, Asefa T, Mesoporosity and Functional Group Dependent Endocytosis and Cytotoxicity of Silica Nanomaterials. *Chem Res Toxicol.*, 2009; 22(11): 1869-1880.